Ejection of fast electrons following the impact of 45 MeV/u $^{58}Ni^{q+}$ ($q=19,28$) on solid-foil targets

G. Lanzanò,[1] E. De Filippo,[1] D. Mahboub,[2] H. Rothard,[3] S. Aiello,[1] A. Anzalone,[2] S. Cavallaro,[2] A. Elanique,[2] E. Geraci,[2] M. Geraci,[1] F. Giustolisi,[2] A. Pagano,[1] and G. Politi[1]

[1]*Istituto Nazionale Fisica Nucleare and Dipartimento di Fisica, Corso Italia 57, 95129 Catania, Italy*

[2]*INFN-LNS and Dipartimento di Fisica, Corso Italia 57, 95129 Catania, Italy*

[3]*Centre Interdisciplinaire de Recherche Ions Lasers, CIRIL-Ganil (UMR 6637 CEA/CNRS/ISMRA), Boîte Postale 5133, 14070 Caen Cedex 05, France*

(Received 31 July 2000; published 5 February 2001)

We report absolute cross sections for binary encounter and convoy electron emission. Fast-electron velocity spectra were measured for atomic collisions induced by a 45 MeV/u ^{58}Ni beam impinging on solid targets by means of the multidetector ARGOS in a large angular range (from 1.5° to 165°). Different conducting elemental targets (^{12}C, ^{27}Al, ^{58}Ni and ^{64}Ni, ^{nat}Ag, ^{197}Au) and polystyrene were used. Characteristics of electrons with a velocity close to the beam velocity (convoy electrons) were found to be very sensitive to the incoming charge state of the projectile. Their yield increases with the target atomic number. The yield of binary encounter electrons with a velocity of almost twice the beam velocity at small ejection angles is roughly proportional to the area density of encountered target electrons. The velocity spectra centroids of these electrons are shifted towards lower velocities than predicted by simple two-body relativistic kinematics. Surprisingly, this effect seems to be mostly independent of target material and thickness. With increasing target atomic number, the high-energy tails of the spectra exhibit an unexpectedly large number of very fast electrons. A multiple-scattering mechanism involving multiple collision sequences of electrons between projectile and target atoms is invoked to explain this effect. The data also show evidence for an excess of fast electrons in the backward direction.

DOI: 10.1103/PhysRevA.63.032702 PACS number(s): 34.50.Fa, 79.20.Rf, 25.70.−z

I. INTRODUCTION

Heavy-ion beams at ''intermediate energies'' (≈20 MeV/u<E<200 MeV/u) have extensively been used in nucleus-nucleus interaction studies. On the contrary, very little attention has been paid to the nucleus-electron interaction, a field being at the boundary between nuclear and atomic physics. This is most surprising since ionization is the most fundamental consequence of energetic atomic collisions and it is at the beginning of radiation effects in inert or living condensed matter. Electron emission is thus also an important probe for the interaction of swift ions with solids [1–5]. Specific effects can be observed with swift heavy ions due to the high charge states. This results in high ionization cross sections, strong induced perturbation, and large electronic energy loss. Furthermore, projectile electrons, also in excited states, and the penetration depth-dependent evolution of the ion charge due to capture and loss of electrons have to be taken into account. The knowledge of fast-electron ejection properties at these high projectile energies, like velocity spectra and production cross-section angular distributions, are important for testing basic atomic ionization theories [6]. Furthermore, the application to nuclear physics is quite obvious, since fast electrons are in general a source of disturbance for experimental detection systems, affecting in particular their resolution.

In the forward beam direction, fast electrons are essentially due to two reaction mechanisms. A binary encounter between the incident ion and an atomic electron produces electrons with a maximum centroid velocity of almost twice the projectile velocity v_P. Since electrons are bound to the target nucleus in different shells, the observed distribution of binary encounter (BE) electrons at a fixed angle is a distribution which reflects the initial momentum distribution of the bound electrons of the target (''Compton profile'') [7]. Also, target electrons may be captured or projectile electrons may be lost into low-lying projectile-centered continuum states [8]. These so-called convoy electrons travel with a velocity close to that of the projectile and lead to a cusp-shaped peak in electron spectra.

Studies of BE electron emission at high beam energies above 10 MeV/u are quite scarce [4–6]. Only recently have fast-electron energy spectra been the object of a particular study either by solid-state experimentalists or atomic collision theorists [9–14]. For reviews on swift heavy ion-induced-electron ejection, see, e.g., [4–6,15].

A relativistic theory based on the electron-impact approximation (EIA) has been developed by Jakubassa-Amundsen [10,16]. The basic concept for describing the ejection of binary encounter electrons (BEE) from the target by heavy, highly charged projectiles in a single collision is the quasielastic scattering approximation where ionization takes place via electron transfer to the projectile continuum. At sufficiently energetic collisions, any interaction with the target core during the collision may be neglected and the active electron scatters elastically from the projectile field. The corresponding cross section is then folded with the electron's momentum distribution (Compton profile) in its initial state. Transport of fast electrons traveling through the solid towards the surface was included in the theoretical treatment [14,16].

Experimentally, the velocity and angular distribution of high energy electrons has been studied recently by a time-of-flight (TOF) method with the ARGOS multidetector array in

 ©2001 The American Physical Society

the NAUTILUS scattering chamber at GANIL by Lanzanò *et al.* [13]. A shift of the centroids of the binary encounter electron velocity distribution to lower velocities than expected from ionization theory involving simple relativistic kinematics was observed. These findings are in contrast with experimental studies performed with a different experimental approach (analysis by magnetic deflection of the electrons) [9]. The origin of this observation is still unclear.

Complex three-body dynamics are involved; either so-called one-center or two-center emission phenomena, as described in [6], could explain these velocity shifts. Such effects should then strongly depend on the specific collision system, i.e., the combination of projectile and target. We therefore performed an experiment with different targets: ^{12}C, ^{27}Al, ^{58}Ni, and ^{64}Ni, ^{nat}Ag, ^{197}Au of almost the same area thickness, 300 μg/cm^2, in order to vary the target nuclear charge Z_T while keeping secondary effects connected to electron transport constant as discussed in [12]. Also, the possible dependence on the target thickness (electron transport) was investigated by using seven different carbon targets of 10, 20, 90, 300, 1025, 2000, and 8300 μg/cm^2 thickness. All of theses targets are conductors. In addition, we also used an insulating polystyrene target of 1050 μg/cm^2 thickness.

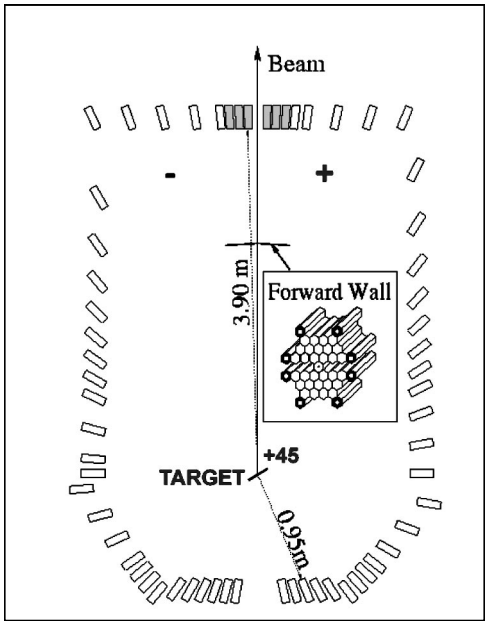

FIG. 1. Sketch of the experimental apparatus, made by a honeycomb-shaped forward wall and an ensemble of 63 (57+6) scintillation detectors positioned in a horizontal plane passing through the center of the target (see text). Positive and negative detector angles are indicated. The target is shown for a tilted angle of +45°.

II. EXPERIMENTAL LAYOUT AND DETECTION METHOD

The experiment was performed at the CS Superconductor Cyclotron of Laboratori Nazionali del Sud (LNS) in Catania, Italy. Pulsed 45 MeV/u 19^+ and 28^+ ^{58}Ni beams with a pulse width (burst time resolution) of 1.2 ns were used. The beam extracted directly from the cyclotron had a projectile charge of $q=19^+$ and was used in a few runs only. Most of the experiment was performed with a bare, $q=28^+$ ^{58}Ni beam, which was obtained by inserting a carbon stripper foil of 2000 μg/cm^2 into the beamline after the extractor. The beam was then charge analyzed and focused on the targets. In most cases, the targets were kept at 0° for perpendicular beam impact. Some runs were also made with the target tilted at 45° with respect to the beam axis.

The experimental layout is shown in Fig. 1. The detection method is very similar to the one described in [13]. The multidetector ARGOS is made of about 100 scintillation detectors (composed of plastic foils of different thicknesses coupled to BaF_2 crystals). Most of these detectors are placed at certain observation angles around the target inside the big scattering chamber CICLOPE of LNS. Additionally, some are mounted in a ''forward wall'' inside CICLOPE to investigate small forward ejection angles. These detectors allow us to identify charged particles, neutrons, and gamma rays from nuclear reactions and also fast electrons. This is done by shape discrimination of the photomultiplier signals (the ''fast'' and ''slow'' components of the detector output) and by measuring the particle time-of-flight as described in detail in [13].

The 30 scintillation detectors placed in the three inner rings of the ARGOS forward wall, at a distance of 2.30 m from the targets at angles of 0.75° to 5.25°, were used to detect nuclear reaction products. No detectors were placed in the horizontal plane of this wall. In this way, the detection of nuclear reaction products and, in particular, electrons with more precision due to a longer flight path for the time-of-flight measurement was made possible. This was achieved with a further battery of six detectors placed in the horizontal plane at a larger distance to the center of the targets of 3.9 m at angles of 1.5°, 3.0°, 4.5° and −1.5°, −3.0°, and −4.5°, respectively (forward shadowed detectors in Fig. 1).

The surface of the hexagonal scintillation detectors measures 25 cm^2. Only the six detectors at large distance were covered by 5-mm-thick aluminum collimators with a circular hole in the middle (radius 1 cm). They worked in the ''inclusive'' mode with a proper electronic divider and were used also for normalization.

The remaining 65 scintillation detectors were used for electron detection only, and their detection thresholds were adjusted accordingly as described in [13]. Fifty-seven of them were placed in the horizontal plane passing through the center of the target at both sides with respect to the beam direction in angular steps of ≈2.5° (see Fig. 1). Eight were placed in the outer ring of the forward wall (black hexagons in Fig. 1). All of them were covered with a 40 μm-thick aluminum collimator, with a circular hole of 1-cm radius in the middle. This reduced the electron count rate by nearly a factor of 8. Unfortunately, this also gave rise to an undesired effect, as the aluminum foil was not thick enough to stop the most energetic electrons completely (≈100 keV) at the most forward angles. Approximately 15% of these electrons were transmitted through the foil with the same time of flight, but with a reduced energy. This effect could be reproduced by

means of an electron transport calculation. This resulted in a reduced fast or slow component, so that for most of the forward detectors the BE electrons were characterized by two loci, almost equally intense, in a fast component time-of flight bidimensional representation (compare Figs. 1 and 2 of Ref. [13]).

To reduce the acquisition rate, these detectors worked only in coincidence with the forward wall, and were divided in three groups. The first (forward) group had 18 detectors including the eight placed in the outer ring of the ARGOS forward wall at 6° and 2.30 m from the target. The remaining ten were at different angles between 6° and 25° at a distance from the target of nearly 4 m. The second (intermediate) group had 22 detectors and covered the angular range between 27.5° (2.65 m from the target) and 90° (1.21 m from the target). The third (backward) group had 25 detectors and covered the angular range between 95° (1.49 m from the target) and 170° (0.92 m from the target). For each of the targets, three separate runs were made with each one of these groups in coincidence with the 30 detectors of the forward wall, and with the six forward detectors working in an inclusive mode. Separate inclusive runs were also made for some selected detectors. In the present experiment, we used a plastic scintillator thickness of 700 μm for the forward wall and the forward group, a variable thickness from 700 to 30 μm for the second group, and 30 μm for the backward group.

III. CHARGE STATE AND TARGET MATERIAL DEPENDENCE

Let us first consider the shape of the electron velocity spectra for the two different charge states as shown in Fig. 2 ($q=19$) and Fig. 3 ($q=28$). Forward spectra are shown for different targets (as indicated) taken at 6°. The electronic threshold was set low enough to also allow the detection of electrons around and below beam velocity. As can be seen from Fig. 2, in the case of a 19^+ beam, the spectra present the following features. The convoy to BE peak ratio is independent of the target atomic number. However, by increasing the target nuclear charge from the carbon to gold target, the spectra show a filling up in the region of velocity intermediate between the beam velocity and the BE velocity. The centroids of the convoy and BE peaks do not depend on the target material. Surprisingly, an unexpected amount of very fast electrons are present in the high velocity tail of the spectrum for the gold target only. The same features are observed with the completely stripped $q=28^+$ ^{58}Ni ion beam (Fig. 3). There is, however, one exception: the relative intensity of convoy and BE electrons now does depend on the target material.

Backward electron velocity spectra, taken at an emission angle of $-140°$ with a $q=28$ charged-ion beam are shown in Fig. 4 for C, Al, Ni, Ag, and Au targets. In particular, one observes a broad distribution which decreases for electron velocities larger than the projectile velocity. The overall intensity increases strongly with the target atomic number Z_T. We show the integrated intensities of forward-emitted BE and convoy electrons, and of backward-emitted electrons as a function of the target atomic number in Fig. 5. The carbon

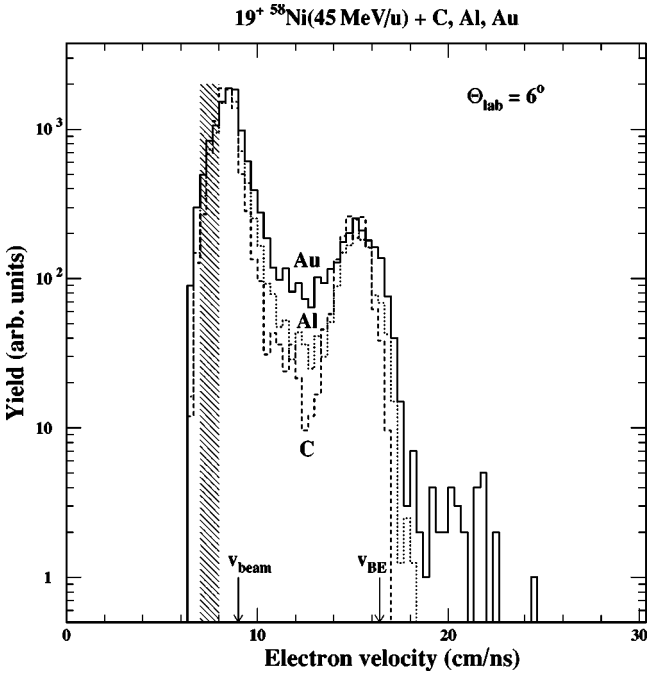

FIG. 2. Electron velocity spectra for the reactions 19^+ ^{58}Ni (45 MeV/u$+$ ^{12}C, ^{27}Al and ^{197}Au, at 6°, normalized to the maximum of the binary encounter peak. The beam velocity and the expected electron velocity for a relativistic binary elastic encounter are also indicated. The electronic threshold is indicated by the shadowed area (≈8–9 cm/ns).

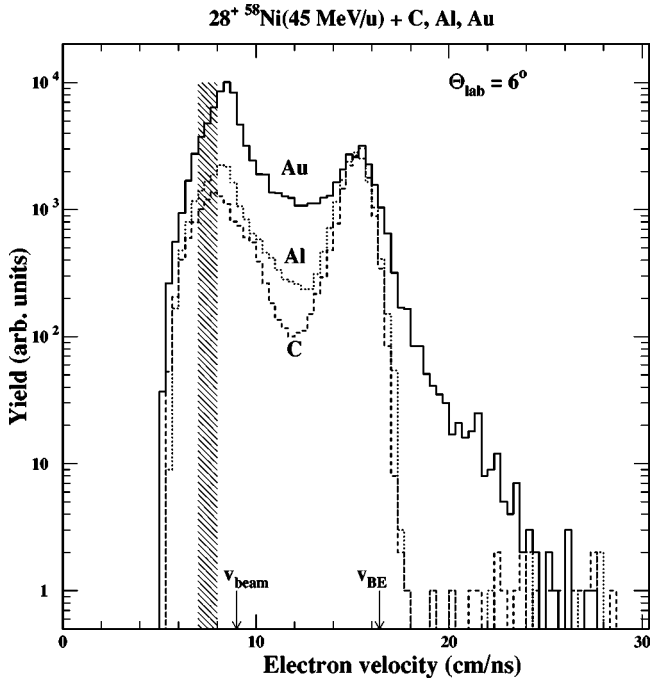

FIG. 3. Same as Fig. 2, but for the reactions 28^+ ^{58}Ni (45 MeV/u$+$ ^{12}C, ^{27}Al, and ^{197}Au at 6°, normalized to the maximum of the binary encounter peak. To get better statistics in the high-energy tail region, we have summed the spectra of the eight detectors at 6° on the forward wall (distance 230 cm to the target) for each target. The beam velocity and the expected electron velocity for a relativistic binary elastic encounter are also indicated. The electronic threshold is indicated by the shadowed area (≈8–9 cm/ns).

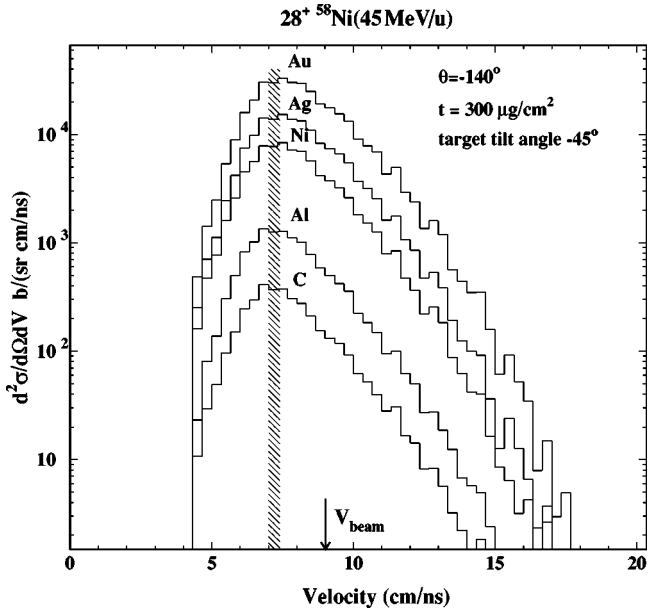

FIG. 4. Backward electron velocity spectra for the reactions 28^+ ^{58}Ni (45 MeV/u)+ ^{12}C, ^{27}Al, ^{28}Ni, ^{47}Ag, and ^{197}Au, at $-140°$. The target, ($\approx$300 μg/cm^2) was tilted at $-45°$ with respect to the beam axis. The beam velocity is indicated by the arrow. The electronic threshold is indicated by the shadowed area ($\approx$7–8 cm/ns).

target thickness dependence of forward-emitted BE electrons is reported in Fig. 6. The cross sections are given per target electron, i.e., per electron area density as discussed in [12].

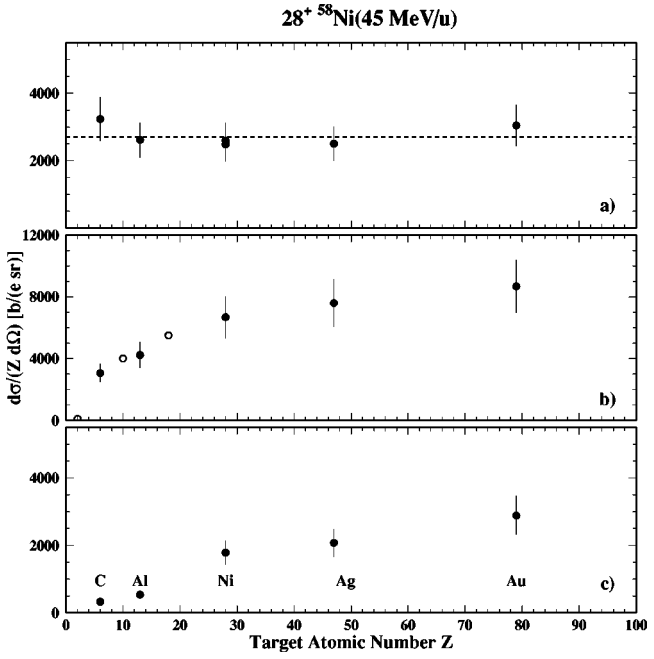

FIG. 5. The absolute yield of forward-emitted binary encounter and convoy electrons, and of backward-emitted electrons ($v_e > 7.3$ cm/ns) induced by 28^+ ^{58}Ni (45 MeV/u) as a function of the target atomic number, respectively in (a), (b), and (c). Data obtained by Breinig *et al.* [8] with swift Ar ions and He, Ne, and Ar targets (open circles, normalized to our data) are included for comparison.

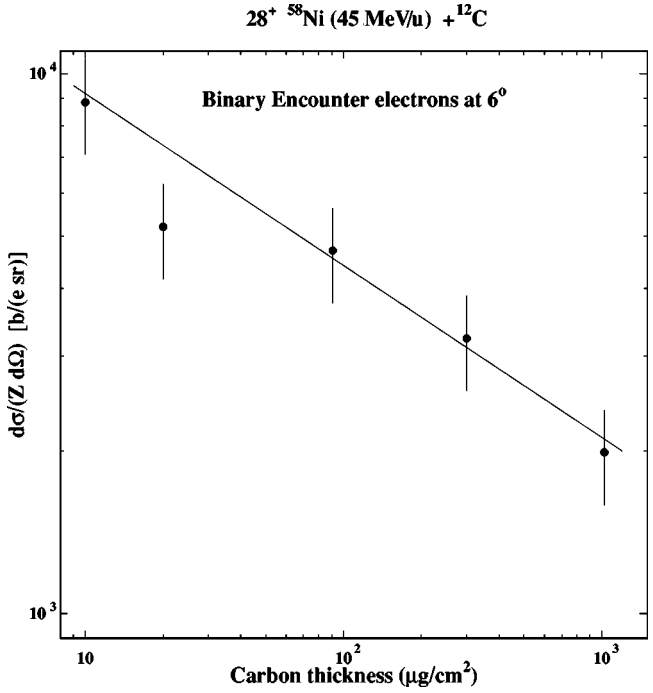

FIG. 6. The absolute yield of forward-emitted binary encounter electrons induced by 28^+ ^{58}Ni (45 MeV/u) as a function of the carbon target thickness. The line is to guide the eye only.

Note that the measured cross sections shown in Figs. 5 and 6 are absolute.

As a function of the target atomic number Z_T, the yield of binary encounter electrons is almost constant within error bars (upper part of Fig. 5). This means that the BE intensities are roughly proportional to the number of electrons ''seen'' by the projectile on its way through the target, i.e., to the number of electrons per unit area. More precisely, one would have to sum over the relative contributions of electrons from different shells, taking into account the electron density and probability of ionization corresponding to each shell. This probability scales roughly with the inverse cube of the binding energy of the electrons, i.e., with E_B^{-3} [17]. We also observe that the normalized yield of BE electrons decreases with target thickness (Fig. 6). This is a transport effect. More and more electrons are scattered out of the detection volume and into large emission angles. We also mention that the BE yield does not depend on the incoming charge state. This result can be understood qualitatively. High-energy BE electron ejection takes place at low-impact parameters so that the incoming charge state only plays a minor role [14]. The result of this binary encounter is then the production of electrons with velocity given approximately by a $2v_P \cos\theta$ behavior as a function of the laboratory angle θ. Except for the velocity shift as discussed below, this is what is observed experimentally (compare also Fig. 4 of [13]). As can be seen from Fig. 7, the angular dependence of the cross section is compatible with a $1/\cos^3\theta_L$ law, as expected [9,12,13,15].

Concerning convoy electrons, threshold effects prevent us from a complete determination of their velocity spectrum, in particular at the low-energy side. Therefore, we calculated the convoy electron yield as two times the peak area inte-

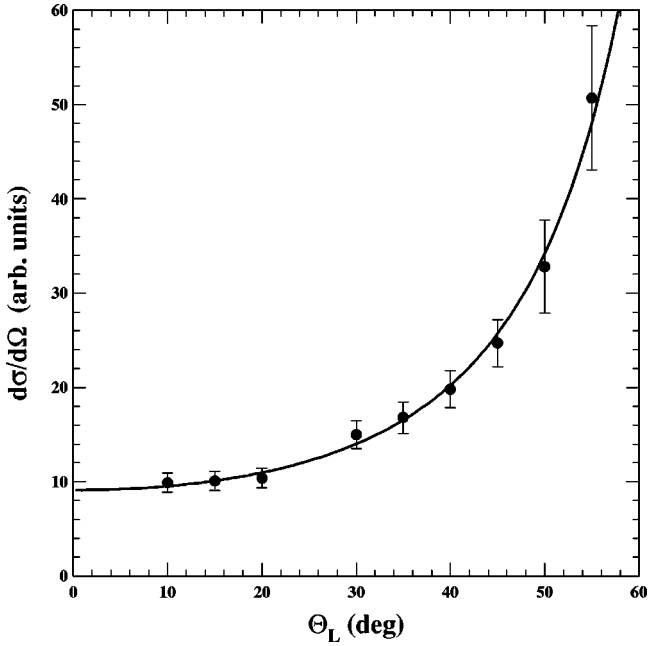

FIG. 7. The high-velocity binary encounter electron-emission cross section is reported as a function of the laboratory detection angle. The line represents the function const/$\cos^3\theta_L$. The reaction is 19^+ ^{58}Ni(45 MeV/u)+ ^{12}C. Error bars take into account both threshold effects and statistics.

grated from projectile velocity up to higher velocities. This part of the spectrum is above the region where threshold effects come into play and can thus be easily evaluated in a consistent way for the different targets. However, for the lightest target (carbon) with fully stripped 28^+ ^{58}Ni beam, the presence of the cusp peak is hardly—if at all—detectable. The convoy electron yield increases with the target atomic number Z_T for the bare ion beam $q=28$. For the $q=19$ beam, the convoy electron intensity remains roughly constant as can be seen from Fig. 2. In this latter case, most of them come directly from the loss of projectile electrons. Here, the projectile is complex and consists of a nucleus of charge 28^+ with a cloud of nine electrons ''in equilibrium.'' During its transit through the target, one or more processes of ''fragmentation'' of this cloud can occur and some electrons may be released (electron loss). In the other case, $q=28$, the incoming projectile is simple and only consists of the nucleus with no orbiting negative charges. If we remain in the language of nuclear physics, in the dynamical and complex projectile nucleus-target nucleus potential, one or more of the target electrons can ''orbit towards'' the ^{58}Ni nucleus, forming a possible equilibrium (in atomic physics language, we would call this ''electron capture''). In a second step, this process can give rise to ''dynamically emitted'' or ''preequilibrium'' electrons, with a broad distribution centered close to the beam velocity, probably with a flat angular distribution [13] (indirect electron loss). However, at high velocities, the capture cross sections are small compared to loss cross sections. This picture allows us to understand the increase of the convoy electron yield with increasing target atomic number: the cross section for electron capture to the continuum (ECC) increases with Z_T ([8]). For comparison, we included data obtained by Breinig *et al.* [8] with swift Ar ions and He, Ne, and Ar targets in Fig. 5. The evolution of both data sets with Z_T is in good agreement.

IV. BINARY ENCOUNTER ELECTRON PEAK SHIFT

Another very important result concerns the position of the BE peak in the forward direction and its dependence on target material and thickness. If we observe carefully Figs. 2 and 3, we note that a slight shift is present between the centroid of the BE peak and the value expected from the two-body relativistic kinematics, as indicated by the arrow [see formulas (1) and (3)]. We have carefully analyzed more precise results obtained with a forward detector at 4.5°, characterized by the largest possible flight path (4 m). As shown in Fig. 2 of Ref. [28], where the BE electron velocity centroid is reported as a function of the target thickness for the different targets, a very slight decrease of the velocity seems to be apparent with increasing carbon target thickness. This can most probably be explained by transport effects [2,3,14]. For all targets, however, within error bars, we obtain a value around 15.5 ± 0.5 cm/ns, independent of the target atomic number. The observed centroid velocity value is slightly below the value predicted by relativistic two-body elastic collision kinematics [16.5 cm/ns, see Eqs. (1)–(3)]. Models used at lower energies [18] predict shifts depending on the complex two-center target-projectile nucleus potential as thoroughly discussed in [6]. In view of these possible three-body (one- or two-center effects) and their possible dependence on the combined projectile-target system, the present result is surprising, and calls for a systematic study of the projectile dependence of this effect.

V. HIGH VELOCITY TAILS: MULTIPLE COLLISION SEQUENCE CALCULATIONS

Concerning the shape of the BE peak at the high velocity side, as anticipated above (Figs. 2 and 3), we come back to the striking difference in the slope for the two spectra from carbon (or aluminum) and gold targets, respectively. In the case of carbon, the high velocity side of the peak falls down very sharply extending up to 17–18 cm/ns with an intensity of almost 1/1000 of the BE peak maximum intensity. In the case of gold, we observe an extended tail which tends to flatten. It extends up to velocities as high as 24–25 cm/ns with the same relative intensity as before. This behavior, peculiar of the gold target, is observed for all other angles up to 60°, as shown in Fig. 8. Such a high-energy tail is not observed for any of the other targets of comparable thickness, not even for the silver or the thicker carbon targets, as shown in Fig. 9.

This can only partly be due to the very complex Compton profile for the gold target. An additional possible mechanism involves multiple collision sequences of electrons between target and projectile nuclei, already invoked to explain high-energy cosmic rays [19,20] or anomalous fusion cross sections in atomic cluster collisions [21,22], and more recently also to account for energetic electrons observed in low-energy ion-atom collisions [23,24].

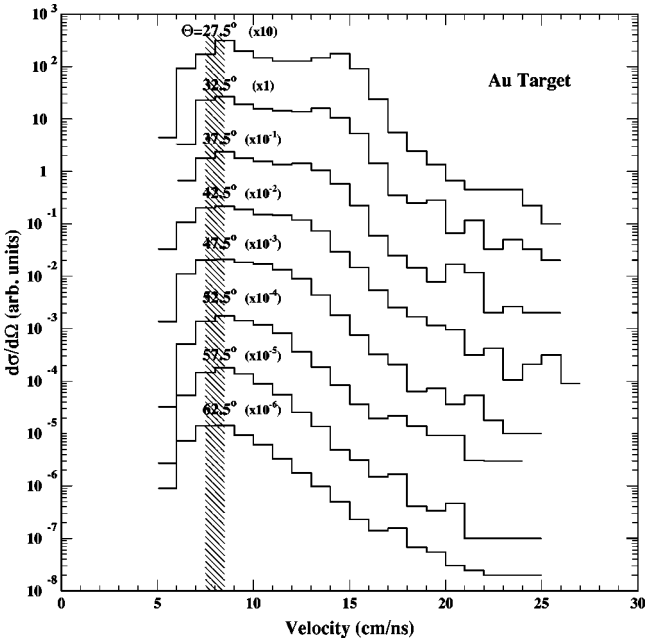

FIG. 8. Electron velocity spectra for the reactions 28^{+} ^{58}Ni (45 MeV/u) + ^{197}Au as a function of the emission angle as indicated. The shadowed area indicates the experimental electronic threshold (≈8–9 cm/ns).

Either remaining projectile electrons or ejected target electrons can undergo multiple collision sequences between the target and incoming projectile nuclei. We emphasize that the probability of such higher-order processes may be sharply enhanced in ion-solid collisions compared to ion-atom collisions because of the high target nucleus density. Electron velocities of up to $3v_P$ and $4v_P$ can be achieved in triple-scattering events. This becomes clear from Fig. 1 of Ref. [22]. A part of the binary encounter electrons produced in the collision interacts with the target atoms along the ion trajectory. Possibly, they are scattered back with a certain velocity distribution, and with a certain probability of colliding again with the same incident nucleus. This simplest process, a double scattering by first the projectile (BE) and then the target, has recently been unambiguously identified even in a heavy-ion–single-atom collision [25,26]. This probability increases strongly the heavier the target and/or the projectile is.

We have calculated the velocity distribution of electrons emitted in forward direction from an elastic collision between a projectile nucleus traveling through the target with a velocity v_P and a backward emitted electron with a collinear velocity $-v_e$ by means of a Monte Carlo procedure. As a first approximation for the velocity distribution of these backscattered electrons we have used the distribution measured at the largest possible backward angle (165°). These spectra closely resemble those shown in Fig. 4: due to threshold effects, this velocity spectrum is essentially an exponential tail starting from 8 cm/ns and extending up to ≈15 cm/ns (see Fig. 4). The excess of fast electrons at backward angles has already been stressed in [13] and is confirmed in the present experiment.

Following the experimentally observed backward spectra, a velocity distribution of the form $Yield = ke^{-av_e}$'' was used as input in the Monte Carlo calculation, k being a normalization constant. In order to obtain the forward ''multiple collision sequence'' component of the electron velocity spectrum, two-body relativistic kinematics for the energy of the outgoing electrons as given by the formulas in [27] was used. We have used the following relativistic formula for the energy of the outgoing electron (projectile) at an angle θ_e (θ_P) in the laboratory system:

$$E_e = \frac{A_{2e}E_T + (p_T c)\cos(\theta_e)\sqrt{A_{2e}^2 - 4E_{0e}^2[E_T^2 - (p_T c)^2\cos^2(\theta_e)]}}{2[E_T^2 - (p_T c)^2\cos^2(\theta_e)]}. \tag{1}$$

Here E_e (E_P) is the total energy, mass+kinetic, for the electron (projectile) after the elastic collision. $E_T = E_e + E_P$ and $p_T = p_e + p_P$ are the total energy and linear momentum, respectively, for the system of the two particles. $E_{0e} = m_{0e}c^2$ ($E_{0P} = m_{0P}c^2$) is the rest mass energy for the electron (projectile) and $A_{2e} = E_T^2 - (p_T c)^2 - (E_{0P}^2 - E_{0e}^2)$ [$A_{2P} = E_T^2 - (p_T c)^2 + (E_{0P}^2 - E_{0e}^2)$]. We have then extracted the electron velocity from the two following formulas:

$$T_e = E_e - m_{0e}c^2 \tag{2}$$

and

$$v_e = c\,\frac{\sqrt{\dfrac{T_e}{m_{0e}c^2}\left(2 + \dfrac{T_e}{m_{0e}c^2}\right)}}{1 + \dfrac{T_e}{m_{0e}c^2}}\ \text{cm/ns}. \tag{3}$$

We recall that classically, for the limiting case of two particles of mass m_1 and m_2 with $m_1 \gg m_2$ and $\theta_1 = \theta_2 = 0$, Eq. (1) reduces simply to

$$v_1 \approx u_1, \quad v_2 \approx 2u_1 - u_2, \tag{4}$$

where u_1 (u_2) is the velocity of particle 1 (2) before the collision. It is clear from Eq. (4) that if u_2 is negative v_2 can

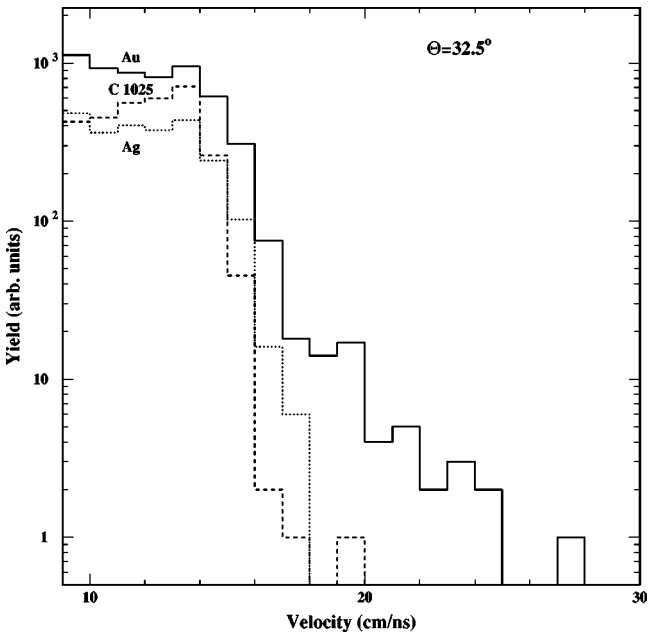

FIG. 9. Electron velocity spectra for the reactions 28^{+} ^{58}Ni(45 MeV/u)+ ^{12}C, ^{27}Al, and ^{197}Au at 32.5°. The target thicknesses are approximately 1000, 300, and 300 μg/cm^2, respectively.

reach values higher than twice the projectile velocity, while the projectile keeps approximately its velocity.

The velocity v_e was varied from 2 to 16 cm/ns. The complete high velocity electron distribution was obtaind by summing the ''multiple collision sequence'' component (multiplied by the normalization constant k) to a fixed Gaussian distribution centered around the experimental BE centroid at 6°. The exponent a was adjusted from a fit of the new velocity distribution to the high velocity part of the measured spectrum at 6°. In this simple calculation, we did not take into account resolution effects nor the fact that electrons could collide with the ingoing nucleus in a noncollinear way. This procedure accounts only for the high velocity part of the tail. Experimental backward-emitted electron spectra present threshold effects below about 7 cm/ns. It is, however, rather the high-energy part of the spectra (see, e.g., Fig. 4) that determines the very-high-energy wing of the calculated forward distribution as shown in Fig. 10, so that the influence of such threshold effects is of minor importance. The results are shown in Fig. 3 of Ref. [28] for $\Theta=6°$. The ''multiple collision sequence'' component fits quite well the experimental tail with $1/a \simeq 3.0$ cm/ns, with an area of $\approx 0.5-1\%$ of the BE peak. We have extended the calculations for other angles, by using the same method with the same value for the a parameter and taking into account the time-of-flight resolution. A general agreement was obtained between the calculations and the experimental spectra. An example is shown in Fig. 10 for the electron velocity spectra at 27.5° and 52.5°.

VI. CONCLUSION

In conclusion, we measured absolute fast-electron ejection cross sections at ''intermediate'' projectile energies.

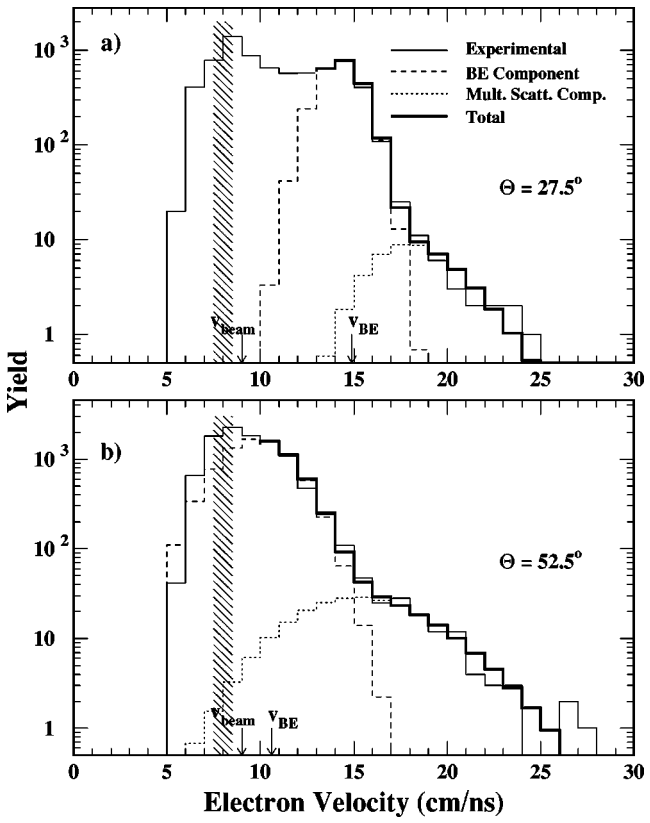

FIG. 10. Electron velocity spectra for the Au target at two different laboratory angles, 27.5° and 52.5°, respectively in (a) and (b) (thin line) in comparison with the prediction of a Monte Carlo simulation, based on a simple two-step multiple collision sequence mechanism (high velocity, dotted line, see text). The Gaussians fitting the BE peaks (dashed line) are also shown. For the high velocity part of the spectrum, the sum of the Gaussian BE component and the multiscattering component is also shown (thick line). The beam velocity and the expected electron velocity for a relativistic binary elastic encounter are indicated by arrows. The shadowed area indicates the experimental electronic threshold (≈8–9 cm/ns).

Electrons from different production mechanisms can serve as probes for different aspects of ion-solid interactions. BE electrons from thin foils probe the very first consequence of such interactions, that is the event of primary ionization. Already at this stage, ''high charge effects'' (deviations from first-order theory, multiple ionization) and the complex dynamics of electrons within the combined (screened non-Coulomb) projectile-target potential render this phenomenon very complicate. Then, with increasing target thickness, transport effects also come into play. Convoy electrons ''feel'' the neighborhood of the moving ion and may serve as a probe of the positively charged wake ''just behind'' the moving ion in insulators. However, we did not observe a striking difference in the electron spectra with an insulating target. Effects on convoy electron emission due to a lens focussing effect by the charged wake of heavy ions in insulating targets were reported [29]. On the other hand, we found that the convoy component of forward electron spectra strongly depends on the incoming projectile charge state.

At the most forward angles, the centroid of the binary encounter electron velocity peak follows a law of the type: $v(0°)\cos\theta$ [13], but $v(0°)$ is ≈10% lower than the value predicted by a two-body relativistic elastic collision kinematics. The value of $v(0°)$ is hardly dependent on the target material and thickness. This feature is in contrast with theoretical expectations based on low-energy experiments [6]. The high-velocity part of the BE peak exhibits an extended tail for heavy targets which can be explained by a multiple collision sequence mechanism: electrons emitted from the primary collision with BE velocity collide again with the projectile after interaction with the target atoms. For the gold target this component amounts to as much as ≈0.5–1% of the BE peak. Furthermore, an excess of fast electrons in the backward direction, as reported in [13], is confirmed in the present experiment.

For BE electron emission at intermediate projectile energies the application of multidetector arrays such as ARGOS, used up to now only in nuclear physics experiments, allow the simultaneous measurement of fast-electron velocity spectra in the entire angular range. This allows us to study fast-electron emission in a very efficient way. Even multiple coincidences (electrons, recoiled atoms, scattered projectiles, and fragments) become possible. In order to understand the observed BE peak shift and the contribution of the multiple collision sequence mechanism to high-enery electron ejection, further studies of the projectile dependence are needed, as well as an extension of the investigated velocity range.

ACKNOWLEDGMENTS

We would like to thank the CS staff for providing the 45 MeV/n ^{58}Ni beam, N. Giudice, N. Guardone, V. Sparti, and S. Urso from INFN, Catania, for helping during the mounting of the experiment, C. Marchetta for target preparation, D. H. Jakubassa-Amundsen and B. Gervais for important discussions, and C. Volant for a careful and critical reading of the manuscript. One of us (H.R.) would like to thank his colleagues at Catania for their hospitality, the INFN-LNS for financial support, and N. Stolterfoht for important discussions.

[1] R.A. Sparrow, R.E. Olson, and D. Schneider, J. Phys. B **25**, L295 (1992); **28**, 3427 (1995).
[2] D. Schneider, G. Schiwietz, and D. DeWitt, Phys. Rev. A **47**, 3945 (1993).
[3] G. Schiwietz, J.P. Biersack, D. Schneider, N. Stolterfoht, D. Fink, V.J. Montemayor, and B. Skogvall, Phys. Rev. B **41**, 6262 (1990).
[4] G. Schiwietz, in *Ionization of Solids by Heavy Particles*, edited by R.A. Baragiola (Plenum, New York, 1993).
[5] H. Rothard, Scanning Microsc. **9**, 1 (1995).
[6] N. Stolterfoht, R.D. Dubois, and R.D. Rivarola, *Electron Emission in Heavy-Ion-Atom Collision*, Springer Series on Atoms and Plasmas Vol. 20 (Springer, Berlin, 1997).
[7] F. Bell, H. Böckl, M.Z. Wu, and H.-D. Betz, J. Phys. B **16**, 187 (1983).
[8] M. Breinig *et al.*, Phys. Rev. A **25**, 3015 (1982).
[9] B.D. De Paola, Y. Kanai, P. Richard, Y. Nakai, T. Kambara, T.M. Kojima, and Y. Awaya, J. Phys. B **28**, 4283 (1995).
[10] D.H. Jakubassa-Amundsen, J. Phys. B **30**, 365 (1997).
[11] T. Azuma *et al.*, Nucl. Instrum. Methods Phys. Res. B **132**, 245 (1997).
[12] H. Rothard, D.H. Jakubassa-Amundsen, and A. Billebaud, J. Phys. B **31**, 1563 (1998).
[13] G. Lanzanó, E. De Filippo, S. Aiello, M. Geraci, A. Pagano, Sl. Cavallaro, F. Lo Piano, E.C. Pollacco, C. Volant, S. Vuillier, C. Beck, D. Mahboub, R. Nouicer, G. Politi, H. Rothard, and D.H. Jakubassa-Amundsen, Phys. Rev. A **58**, 3634 (1998).
[14] D.H. Jakubassa-Amundsen and H. Rothard, Phys. Rev. A **60**, 385 (1999).
[15] H. Rothard, Nucl. Instrum. Methods Phys. Res. B **146**, 1 (1998).
[16] D.H. Jakubassa-Amundsen, Phys. Scr. **T80**, 252 (1999).
[17] G.N. Ogurtsov, Rev. Mod. Phys. **74**, 1 (1972).
[18] P.D. Fainstein, V.H. Ponce, and R.D. Rivarola, Phys. Rev. A **45**, 6417 (1992).
[19] E. Fermi, Phys. Rev. **75**, 1169 (1949).
[20] P.L. Biermann, J. Phys. G **23**, 1 (1997).
[21] C. Carraro, B.Q. Chen, S. Schramm, and S.E. Koonin, Phys. Rev. A **42**, 1379 (1990).
[22] M. Hautala, Z. Pan, and P. Sigmund, Phys. Rev. A **44**, 7428 (1991).
[23] S. Suarez, G. Bernardi, P. Focke, W. Meckbach, M. Tobisch, M. Jung, H. Rothard, M. Schosnig, R. Maier, A. Clouvas, and K.O. Groeneveld, Nucl. Instrum. Methods Phys. Res. B **86**, 197 (1994); see also S. Suarez, R.O. Barrachina, and W. Meckbach, Phys. Rev. Lett. **77**, 474 (1996).
[24] B. Sulik, Cs. Koncz, K. Tőkési, A. Kövér, S. Ricz, GY. Vikor, J.-Y. Chesnel, N. Stolterfoht, and D. Berényi, Nucl. Instrum. Methods Phys. Res. B **154**, 281 (1999).
[25] U. Bechthold, S. Hagmann, J. Ullrich, B. Bathelt, A. Bohris, R. Moshammer, U. Ramm, C. Bhalla, G. Kraft, and H. Schmidt-Böcking, Phys. Rev. Lett. **79**, 2034 (1997).
[26] C.O. Reinhold, D.R. Schultz, U. Bechthold, G. Kraft, S. Hagmann, and H. Schmidt-Böcking, Phys. Rev. A **58**, 2611 (1998).
[27] A.M. Baldin, V.I. Gol'danskii, and I.L. Rozenthal, *Kinematics of Nuclear Reactions* (Pergamon, New York, 1961).
[28] G. Lanzanó, E. De Filippo, D. Mahboub, H. Rothard, S. Aiello, A. Anzalone, S. Cavallaro, A. Elanique, E. Geraci, M. Geraci, F. Giustolisi, A. Pagano, and G. Politi, Phys. Rev. Lett. **83**, 4518 (1999).
[29] G. Xiao, G. Schiwietz, P.L. Grande, N. Stolterfoht, A. Schmoldt, M. Grether, R. Köhrbrück, A. Spieler, and U. Stettner, Phys. Rev. Lett. **79**, 1821 (1997).